

Numerical Analyses of a Cavitating Pelton Turbine

Pavesti¹ G. – Rossetti¹ A. – Santolin² A. - Ardizzon¹ G.

¹University of Padova - Department of Industrial Engineering - Via Venezia 1 - 35131 Padova, ITALY

²Tamanini Hydro s.r.l. sal. Dossi 5 - 38123, Mattarello (TN), ITALY

ABSTRACT

Erosive wear of hydro turbine runners is a complex phenomenon, which depends upon many parameters and which leads to a decrease of the performance in time and/or in extreme cases to the rotor mechanical failure. Consistently, the study of this wearing process is an important step to improve the impeller design, to avoid or minimize the rise of extraordinary maintenance.

In the present paper the cavitation mechanics of a Pelton turbine was investigated using CFD analyses. A Pelton affected by pitting cavitation was taken as test case. The Pelton geometry was modelled and analyzed using unsteady Reynolds averaged Navier-Stokes (RANS) multiphase analyses. The homogeneous approach was used to describe the multiphase flow composed by water, water vapour and air.

Numerical results discriminated the vapour production processes during the cut in of the bucket on the water jet. The design and the part load flow rates were analyzed and the cavitation process compared.

A simple procedure to identify the locations of higher damage risk was presented and verified on the test case runner.

NOMENCLATURE

a_{vf}	air volume fraction	[-]
B	bucket width	[m]
d_{jet}	jet diameter	[m]
D_{PCD}	Pitch circle diameter	[m]
H	net hydraulic head	[m]
n	rotational speed	[rpm]
n_b	number of bucket	[-]
P	power	[kW]
Q	flow rate	[m ³ /s]
t	time	[s] or [μs]
t_0	start of the evaluation period	[μs]
$z^* = \frac{z}{d_{jet}/2}$	adimensionalized axial distance	[-]
w_{vf}	water volume fraction	[-]
v_{vf}	vapour volume fraction	[-]
Δt	numerical timestep	[s]
$\Delta t_b = 2\pi / \omega / z_b$	bucket period	[s]
ω	rotational speed	[rad/s]

INTRODUCTION

Cavitation in hydraulic machinery produces instabilities, vibrations, damage to material surfaces and degradation of machine performance. Due to today's growth of the turbine output power and the dimensions reduction, to decrease the cost of the components, the turbine speeds are being increased and the cavitation number is consistently decreased. Moreover, the deregulation of the hydropower generation market forces to operate the turbines in conditions far from their best efficiency point with cavitation phenomena more marked. The combination of both factors is promoting the risk of cavitation problems in hydraulic machines.

Although cavitation within pumps has been the subject of extensive research up to now, few studies have been published related to cavitation within hydropower turbines particularly focused on Pelton.

The unsteady interaction between the buckets and the jet and high fluid velocities and gradients on the bucket surfaces can cause aggressive cavitations on the bucket tip and back during the jet cut process. Furthermore cavitation can occur on the bucket splitter and sides when the bucket is not properly designed.

Limited information can be found documenting the cavitation phenomena on Pelton turbines and often the reference on Pelton Bucket cavitation in the specialized publications [1, 2], is only from the paper of H. Grein [3] even if A. Perrig [4] in 2006 published his PhD thesis where he proposed measurements and a numerical simulation on the issue of cavitation development in Pelton turbines.

Other authors focused on the enhancement of silt erosion caused by the presence of cavitation [5, 6].

The characteristic of unsteadiness and the presence of two different phases and fluids made the CFD approach to Pelton turbine highly computationally expensive when compared to the effort to simulate Francis and Kaplan turbines. Consistently the use of numerical analyses to predict and describe the performance of a Pelton turbine is quite recent. The first analyses were focused on the study of the free surface analyses of the water jet [7-10] and only recently the analyses of the jet bucket interaction and of a full scale runner have been developed ([11-14]).

In this article the cavitation mechanics was investigated by CFD analyses in a Pelton test case affected by pitting cavitation. The bucket geometry was modelled and analyzed using unsteady Reynolds averaged Navier-Stokes (RANS) multiphase analyses. The homogeneous approach was used to describe the multiphase flow composed by water, water vapour and air.

Numerical results allowed to highlight the different vapour production during the water jet cut in processes by the bucket. On the base of the numerical results a simple model to predict the presence of pitting cavitation and to identify the locations of higher damage risk on the buckets was proposed and verified on the test case runner.

TEST CASE

The Pelton under test was a 1000 kW turbine of power plant in the north of Italy working at approximately 950 [m] above the sea level. The turbine is a horizontal axis Pelton turbine, with 21 buckets about 0.184 m width, a Pitch Circle Diameter (PCD) of 0.715 m and 2 injectors. The main turbine data information are reported in Table 1.

The turbine was subject to rapid cavitation erosion on the back of the splitter tip (fig. 1) and, with minor intensity on the back of the cut-out (fig. 1). The damaged surface of the bucket is clearly visible in fig. 1a, whereas fig. 2b shows the damages and the significant alteration of the cut-out edge.

The relative jet paths are reported in fig. 2 for the symmetry section of the reference geometry for the first and the last contact of the splitter tip with the jet. The bucket back profile was designed

Table 1: Pelton test case data

H	310	[m]
Q_{Des}	0.37	[m ³ /s]
P_{max}	1000	[kW]
n	1000	[rpm]
n_b	21	[-]
B	0.184	[m]
D_{PCD}	0.715	[m]
n_i	2	[-]

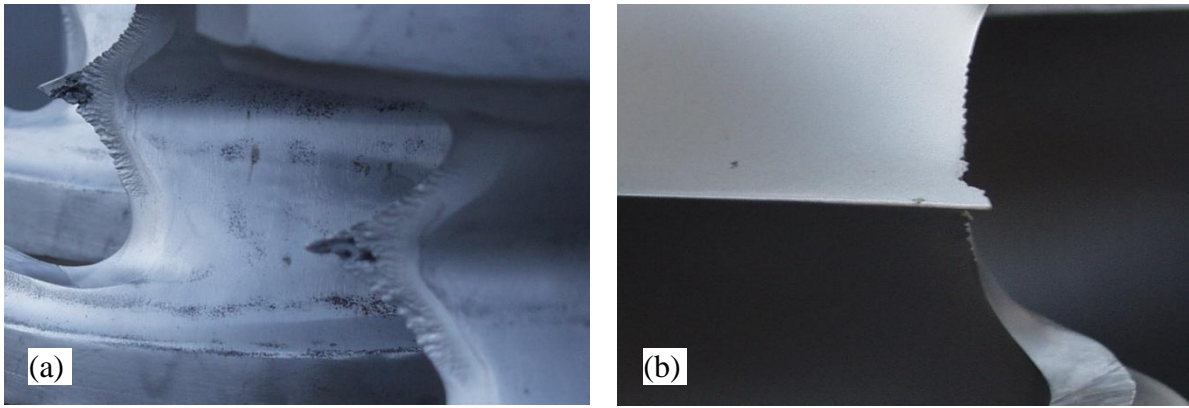


Fig. 1. Cavitation damage on the test case runner; a) cavitation pitting on the splitter tip back; b) front face of the bucket.

to have a relevant interaction between the back and the jet that is with a constructive angle of the profile lower than the flow angles during the whole process and not only in the first cut in stages.

This bucket back profile should avoid the origin of a dynamic depression on the bucket back, in clear contrast with the erosion found on the runner. Consistently the pitting damage causes on the splitter tip back could not be identified only by this simplified approach and CFD analyses were used to identify the mechanics of the cavitation process.

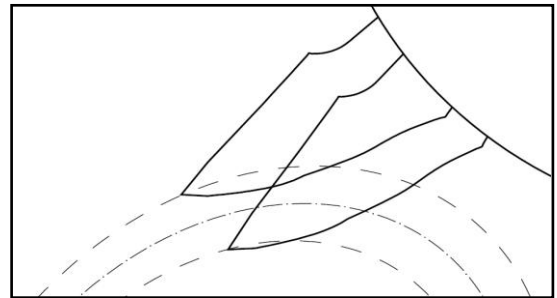


Fig. 2. Relative jet flow and bucket profile on the symmetry plane of the model.

NUMERICAL ANALYSES

Numerical analyses were carried out using the commercial code Ansys CFX 13.0. The nozzle geometry impact on the jet shape was ignored and an ideal jet configuration, perfectly axial symmetric and free from secondary flows, was assumed. To reduce the number of mesh elements, a 3 buckets model of the runner was used instead of the overall 21 buckets configuration. Only the intermediate bucket was used as reference to collect the numerical data, while the modelling of the only previous and following buckets were considered satisfactory to describe the overall interaction between consecutive buckets and the jet.

Only one half of the turbine width was modelled due to the geometrical longitudinal symmetry of the system. The numerical model is shown in fig. 3.

The stationary domain reproduced the casing and the external profile of the nozzle, while the nozzle inner hydraulic profiles were not considered.

To model the ideal jet a free slip wall cylindrical surface was supposed to guide the flow to the nozzle exit and a constant velocity profile in a rear section of the nozzle exit was imposed as inlet condition.

The outlet condition was imposed on the bottom surface of the model, imposing the atmospheric absolute pressure computed considering the height over the sea level of the test case power plant. The bucket surfaces were modelled as no slip hydraulically smooth walls (fig. 3).

The numerical domain was discretized using both hexahedral structured and tetrahedral unstructured meshes. The hexahedral structured mesh was preferred on the stationary domain, where the jet position and velocity direction remain constant in time. The use of hexahedral elements aligned along the jet axis allowed a good refinement on the water–air interface combining high numerical accuracy and mesh quality. On the contrary, the unsteady flow, the absence of a preferred flow direction and the unsteadiness into the rotating domain suggested the use of tetrahedral unstructured mesh into the Pelton runner. Mesh refinements were provided near the bucket surfaces

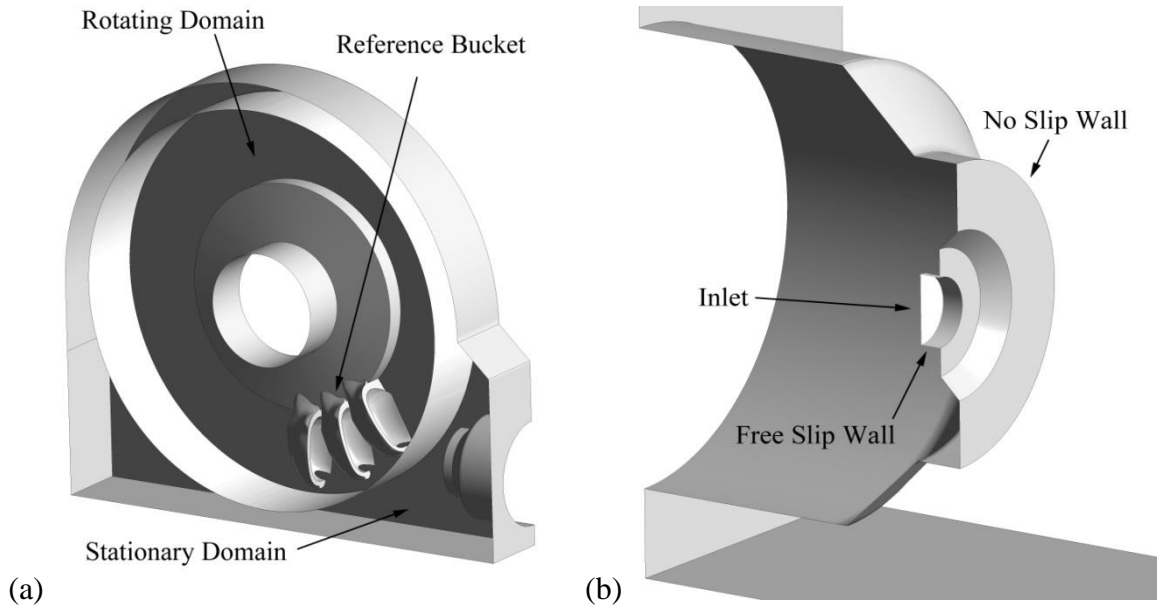


Fig. 3. Numerical domains; a) Rotating and stationary domains; b) detail of boundary condition at the jet inlet.

and near the thin edges such as the splitter and the cut-out. The adopted mesh is shown in fig. 4, while table 2 reports the mesh statistics.

The two phase, three component flow was modelled using an Eulerian–Eulerian model, with the assumption of homogeneous flow. This model should be applied only when no relevant momentum exchange occurs between the phases. The collapse of cavitation bubbles leads to significant exchange in momentum between the vapour and the water but the bubble collapsing time was considered too small and the process too fast to be modelled into a full scale runner. Until no other relevant interaction among air, water vapour and water itself took place inside the domain, the use of a homogeneous model was considered suitable for the cavitation analyses.

Constant property characterizations were adopted for all the three fluids. Standard values were used for the thermodynamic variables, assuming isothermal flow at 25°. The reference state of the considered fluids is reported in table 3.

The Rayleigh–Plesset [15] cavitation model was adopted to model the water – water vapour inter phase transfer. The buoyancy was considered to model the deflexion of the jet mean axis and to promote the discharge of the water from the lower side of the model. Turbulence was modelled using the SST model.

Second order schemes were adopted both for the advection and transient scheme. The simulation time step was based on the bucket passing period that is the time between the passage of two contiguous buckets: $\Delta t_b = 2\pi / \omega / n_b$. Two time steps were tested, a two hundred eightieth of the

Table 2: Mesh statistics

	Stator	Rotor	Total
Number of Nodes	912 061	1 892 493	2 804 554
Element Type	Hexahedral	Tetrahedral	Mixed
Number of Elements	863096	10 823 780	11 686 876

Table 3: Fluids properties

	Water	Water Vapour	Air
Thermodynamic State	Liquid	Gas	Gas
Density [kg m ⁻³]	997.0	0.02308	1.185
Dynamic Viscosity [kg m ⁻¹ s ⁻¹]	8.899e-4	9.8626e-6	1.831e-5
Saturation Pressure [Pa]	-	3141.7	-

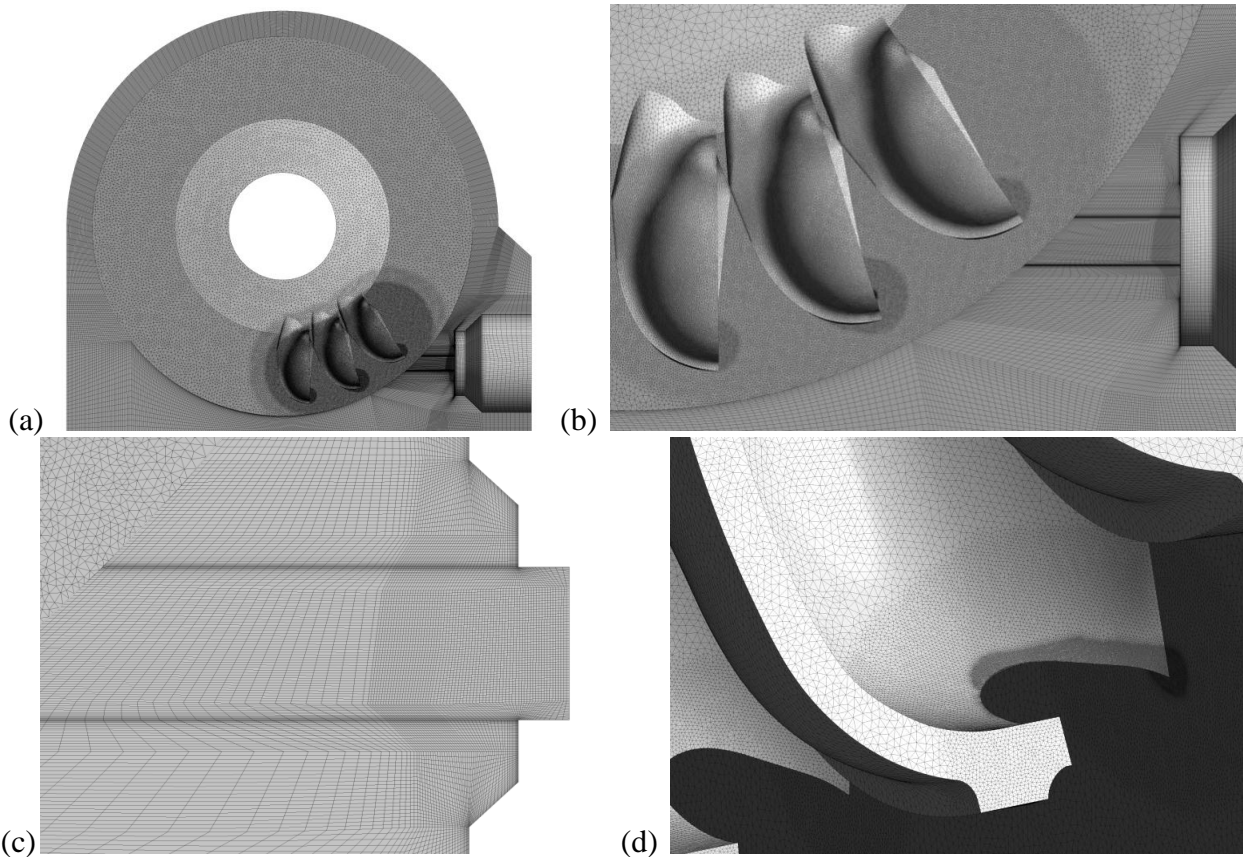


Fig. 4. Numerical model Mesh; a) Sketch of the mesh of the whole numerical model; b) detail of the three bucket and the nozzle; c) detail of the structured mesh on the symmetry plane; d) detail of the refinements on the cut-out of the bucket.

bucket passing period ($\Delta t = 1/280\Delta t_b = 10.2\mu s$) and a five hundred sixtieth of the bucket passing period ($\Delta t = 1/560\Delta t_b = 5.1\mu s$). The vapour volume values and them trend did not change in a remarkable way and consistently the higher timestep was used in the analyses. The higher averaged RMS Courant Number obtained in all the analyses was equal to 0.8.

The maximum number of iterations for each time step was set to be 5, resulting in a water and vapour masses residues of 10^{-6} , momentum residues of 10^{-5} , turbulent kinetic energy and energy dissipation residues of 10^{-5} .

Two flow rates were considered, the design flow rate (reported in table 1) and a part flow equal to the 50% of the design flow rate.

RESULTS

The water vapour volume generated during the cut in process is reported in figs 5 and 6 for flow design and part flow respectively. The origin was referred to the time when the spitter tip first touched to the most inner streamline of the free jet. Both time when the splitter ridge is just at the bottom of the jet that is the full jet entered the bucket and when the cut-in process ends are also reported in the graph.

Vapour production started with a delay in regards to the cut-in and reached its maximum when the splitter ridge of the bucket was just at the bottom of the jet for both the flow rates.

The main fraction of the vapour volume reported in figs 5 and 6 came from the back of the bucket (zone B in fig. 7) and evolved over a relative long time.

In the early stage of the cut-in the jet is attached to the bucket profile and the streamlines are deflected down due the impact of the bucket back on the jet (figs 8a and 9a) consistently with the relative flow paths shown in fig. 2.

As the bucket moved through the jet (figs 8b–8e and 9b-9d), the rear surface interfered with the

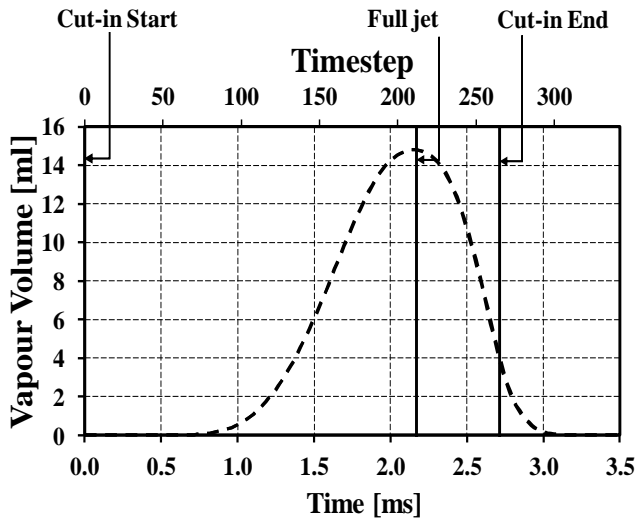


Fig. 5. Water vapour volume versus time around the bucket ($Q = 100\% Q_{Des}$).

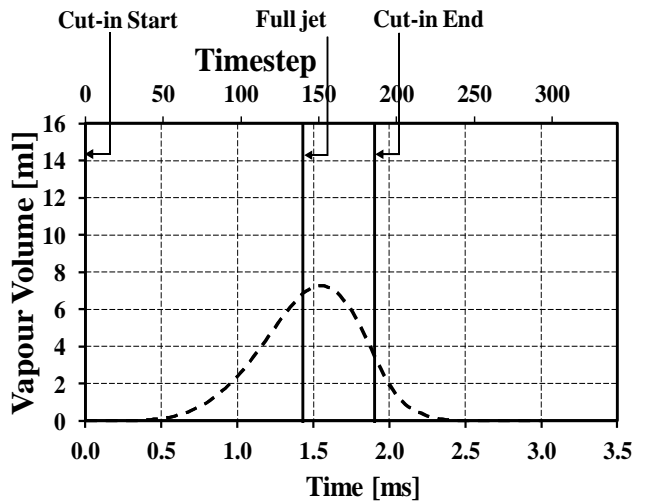


Fig. 6. Water vapour volume versus time around the bucket ($Q = 50\% Q_{Des}$).

flow-off jet speeding up the detachment of the flow from the rear surface. Consistently, the back face of the bucket was depressurized and the water flowing attached to the back face (fig. 8a) isolated a vapour pocket both at the design flowrate (fig. 8b) and at the part load (fig. 9b).

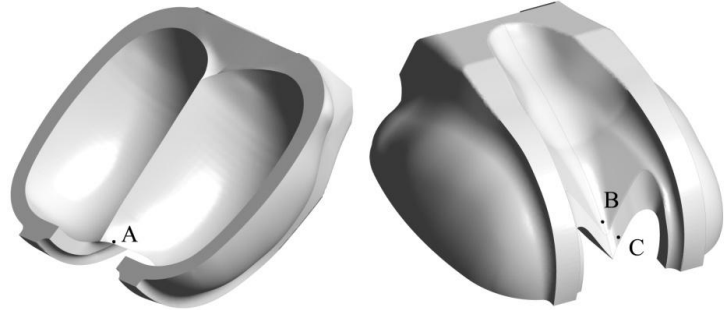


Fig. 7. Location characterized by vapour volume fraction in the CFD model.

When the water departed from the bucket (figs 8c-8d and fig. 9c), the air flowed inside the depressurized volume, scrubbed the water vapour from the bucket surface, and forced it to move stuck to the water jet (figs 8e and fig. 9d).

The sections parallel to the symmetry plane showed an analogous trend but with different time schedules. The external sections showed a delay as it is visible in fig. 10 for the design flow rate, where different sections are compared at the same time. Consistently the maximum water vapour volume was reached when the bucket splitter ridge was at the bottom of the jet (fig. 5) or just later

(a) $t = 0.510$ [ms] (b) $t = 1.041$ [ms] (c) $t = 1.347$ [ms] (d) $t = 1.653$ [ms] (e) $t = 1.857$ [ms]

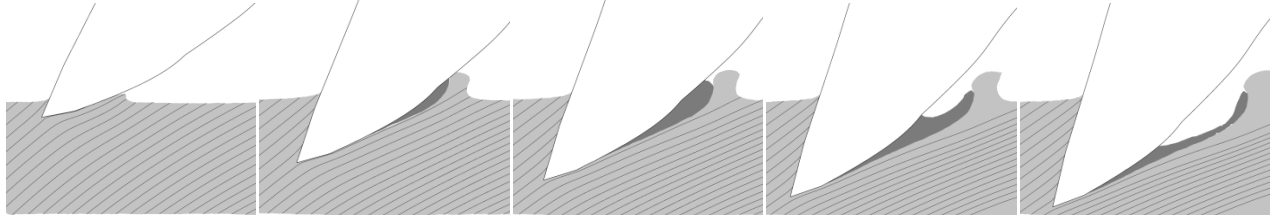


Fig. 8. Relative streamline on the symmetry plane, ■ water, ■ water vapour ($Q = 100\% Q_{des}$).

(a) $t = 0.245$ [ms] (b) $t = 1.020$ [ms] (c) $t = 1.449$ [ms] (d) $t = 1.663$ [ms]



Fig. 9. Relative streamline on the symmetry plane, ■ water, ■ water vapour ($Q = 50\% Q_{Des}$).

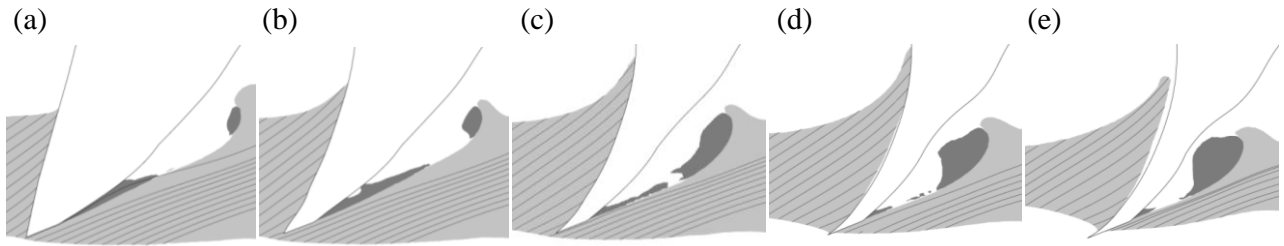


Fig. 10. Relative streamline at $t = 2.06$ [ms] at different planes; a) symmetry $z^* = 0$, b) $z^* = 20\%$, c) $z^* = 50\%$, d) $z^* = 75\%$, e) $z^* = 90\%$, ■ water, ■ water vapour ($Q = 100\% Q_{Des}$).

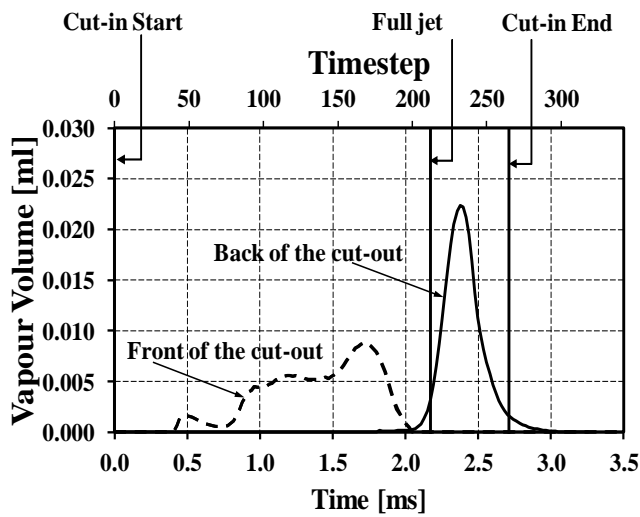


Fig. 11. Time evolution of water vapour volume on the cut-out ($Q = 100\% Q_{Des}$).

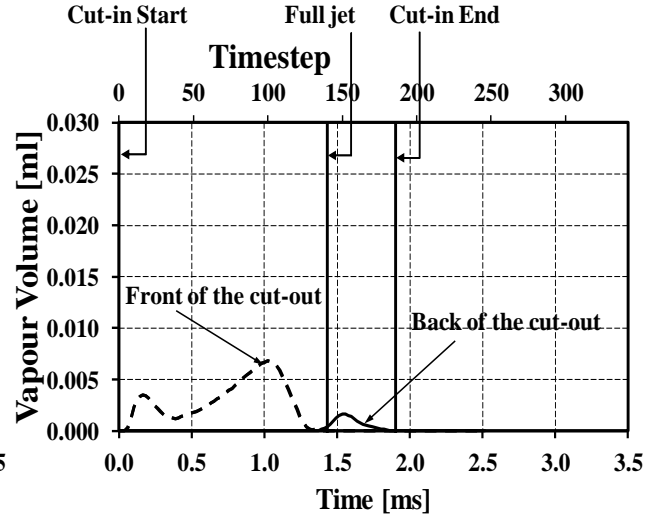


Fig. 12. Time evolution of water vapour volume on the cut-out ($Q = 50\% Q_{Des}$).

(fig. 6).

The vapour generated in the front face of the bucket near the cut-out at the outside end of the splitter (zone A fig. 7) and in the back of the cut-out (zone C fig. 7) is reported in figs 11 and 12.

The front face of the bucket was affected by sheet cavitation in the starting cut in phase. The small amount of vapour production was due to a difference between the relative flow angle and the constructive angle of the cut-out (fig. 13).

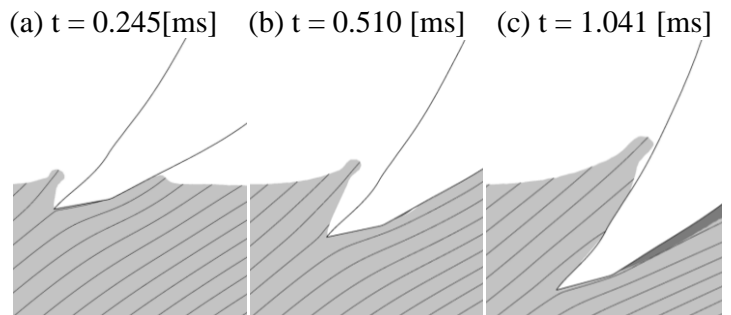


Fig. 13. Relative streamline at different instants in the plane $z^* = 20\%$; ■ water ($Q = 100\% Q_{Des}$).

The jet impact with the bucket back caused the flow detachment from the bucket surface and the progressive reattachment (fig. 13a-c). The vapour was produced in the form of a thin sheet in the detached area near the bucket cut-out and it is shown as a black strip in Fig. 1 for both the flow rates under test.

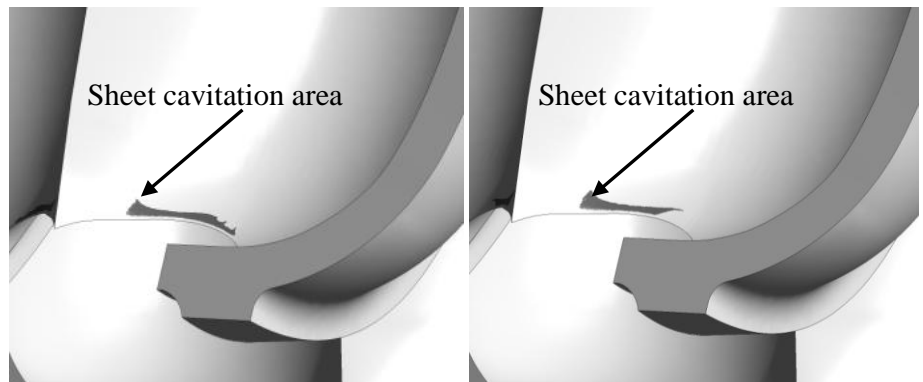
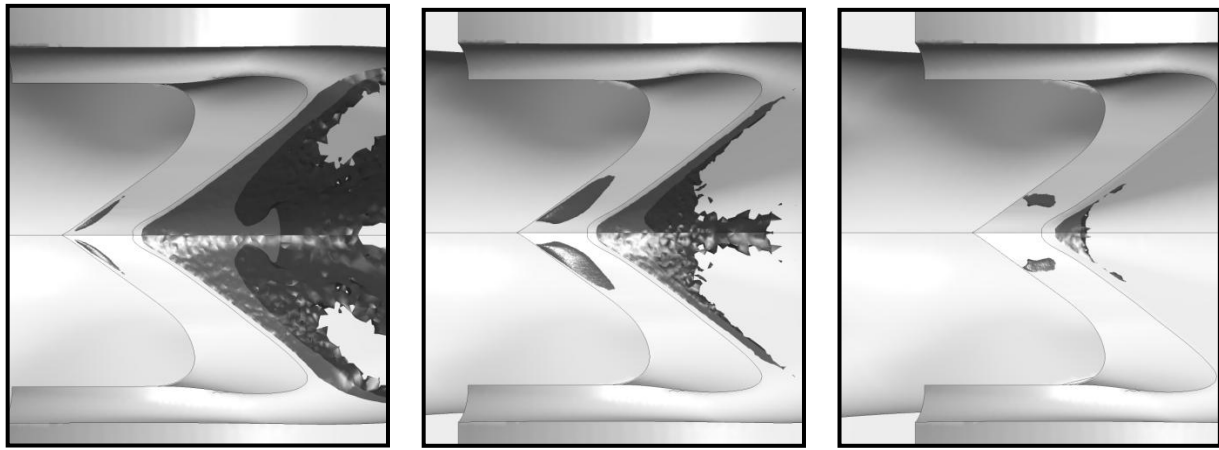
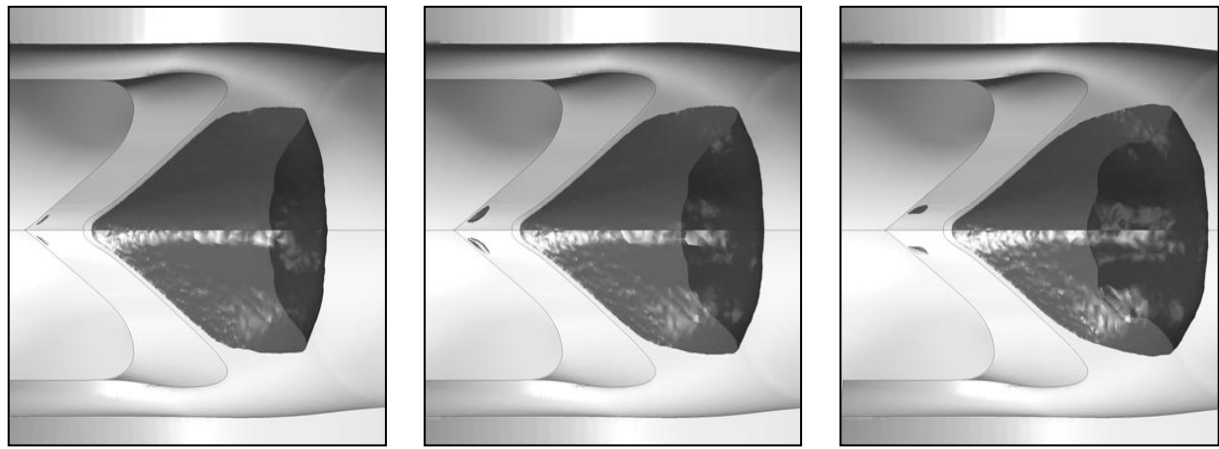


Fig. 14 Sheet cavitation in the front face of the cut-out at design flow rate and part load ($Q=50\% Q_{Des}$)



a) $T = 2.06$ [ms] b) $T = 2.27$ [ms] c) $T = 2.47$ [ms]
 Fig. 15 Development of water vapour for different cut in position ($Q = 100\% Q_{Des}$).



a) $T = 1.449$ [ms] b) $T = 1.531$ [ms] c) $T = 1.633$ [ms]
 Fig. 16 Development of water vapour for different cut in position ($Q = 50\% Q_{Des}$).

Until the genesis of vapour is the same for all the flow rates and the incidence angle substantially does not change with the flow rate, both the amount (figs 11 and 12) and the location (fig. 14) of the vapour volume are quite the same for the two flow rates analysed.

The vapour at the splitter cut – out back took place in the last instants of the cut in process due to the local flow incidence and depression highlighted when the bucket approached the lower surface of the water jet (figs 11 and 12). The vapour was shaped in pockets (figs 15a and 16a), which grew up in the subsequent instants (figs 15b and 16b).

The vapour peak was reached successively the splitter ridge passed through the bottom of the jet (figs 11 and 12). Successively the bucket completes the transit through the jet and the pressure outside the vapour pocket suddenly increased to the atmospheric pressure due to the air entry from the symmetric plane. The increase of local pressure, above the saturation pressure, led to a reduction of the vapour where condensation velocity decreased with the reduction of the flow rate. (figs 11 and 12).

The vapour volume generated was small but differently from the vapour bubbles highlighted in the other two zones, showed locally a highly impulsive trend with the vaporization and collapse phases starting and ending in less than 0.5 [ms] for the two flow rates (figs 11 and 12).

FORECAST OF POSSIBLE CAVITATION PITTING DAMAGE USING VOF CFD ANALYSES.

Cavitation structures carry a significant amount of potential energy [16] and can, at their collapse, emit pressure waves of magnitude of several MPa [17]. Yet it seems that the cavitation

cloud collapse itself cannot be the direct cause of erosion as its energy is not concentrated enough.

Currently the most widely accepted explanation of the phenomenon is that the potential energy contained in a macro cavity (cavitation cloud) is transformed into the radiation of acoustic pressure waves, and further on into the erosive power contained of the micro-scale cavitation structures or single bubbles that implode in the vicinity of the material boundaries. The approach, known as the “multiscale energy cascade”, was first used by Fortes-Patella et al. [17] and Bark et al. [18] to explain the damage occurrence.

Consistently, the post processing of the numerical data allowed to suggest a simplified approach to identify the vapour volume that could damage the rotor.

The regions of possible damage were identified assuming that the surface damage could take place only when the following three main conditions were checked at the same time:

1. the vapour cavity is sticking to the bucket surface;
2. water vapour is condensed in a small time to arise damaging process;
3. the condensation of water vapour is developed in absence of air, otherwise no shocking waves of micro jets could develop.

The last two conditions were synthesized by the following relations to allow a systematic analysis of the possible pitting damage points:

1. $v_{vf}(t) > 0.80$;
2. $v_{vf}(t + \Delta t) < 0.20$ where $\Delta t \leq 40 [\mu s]$;
3. $a_{vf}(t) < 0.10$ for $t_0 < t < (t_0 + \Delta t)$.

The vapour volume fraction thresholds of 0.8 and 0.2 were fixed to identify, unambiguously, the vapour condensing process by the numerical model.

The collapsing time was assumed on the base of a simplification of the governing equations of cavitation dynamics of bubble clouds where all bubbles in the cloud were assumed of equal sized in each time step, heterogeneous bubble interaction was considered and both the influences of circulation and strain on these quantities have been analyzed [20, 21].

The assumed collapsing time (40 $[\mu s]$) is a very long time compared to the collapsing time of a single bubble but long enough to be able to describe the high aggressiveness of cloud cavitation collapse phase. It corresponds to 4 timestep in the numerical analyses, which was found the minimum number of timesteps to complete numerically the phase change from vapour to water.

The vapour and the air volume fraction versus time were monitored on 170 points distributed on the regions affected by the vapour. The points positioned on the front face of the cut-out (zone A

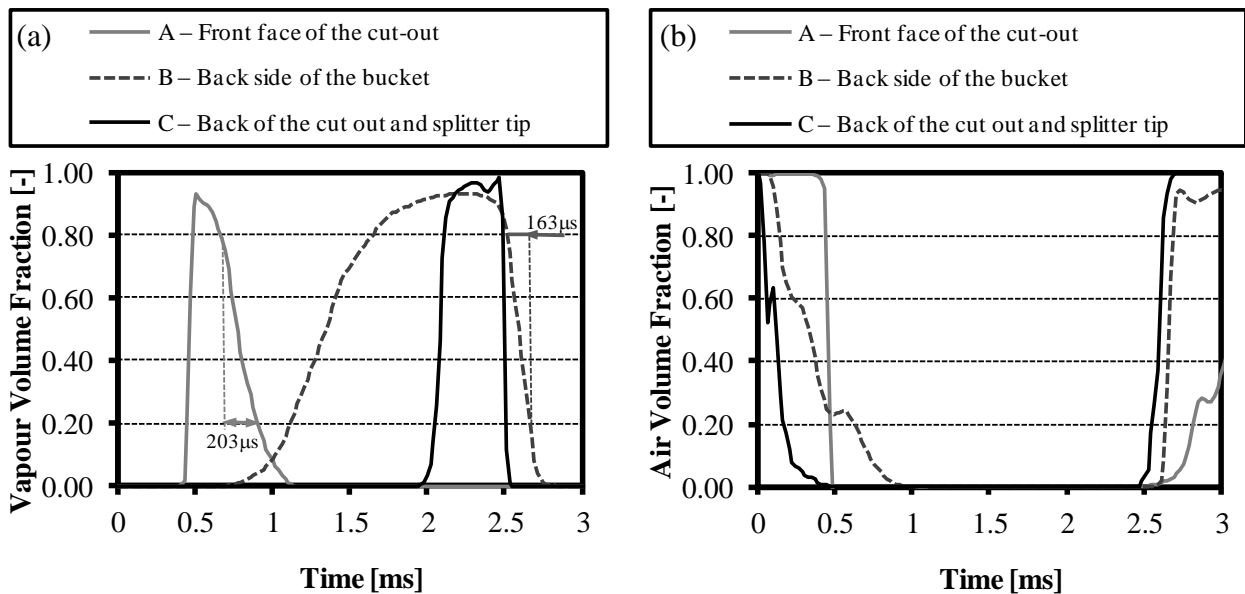


Fig. 17. Vapour (a) and air (b) volume fraction evolution for three points of fig. 6 ($Q = 100\% Q_{Des}$).

fig. 6) presented an impulsive vaporization, but a relatively long time of collapse (~ 203 [μs] at the design flow rate and ~ 163 [μs] at $50\% Q_{\text{Des}}$) for the more critical condition with a quasi – equilibrium transformation of vapour phase to liquid happens (figs 17 and 18).

The points positioned on the back face of the bucket (zone B fig. 6) showed a faster dissolution of the vapour phase, but a significant air fraction was present at the end of the collapse consistently with the previously described scrubbing action of the air. Moreover the collapsing time (~ 163 [μs] at the Q_{Des} and ~ 122 [μs] at $50\% Q_{\text{Des}}$) was excessively long to threaten the bucket integrity (fig. 1).

The three constraints were fulfilled by the points positioned on the cut-out back (zone C fig. 6) at the design flow rate (fig. 17). The vapour collapse was highly impulsive, while the air fraction was very low (less the 5%) (fig. 17). The points which fulfilled in a stricter way the assumed constraint are, shown in fig. 19 and they are all located in the area where the pitting effect is more marked (fig. 1) and the more critical conditions were obtained closer the splitter tip consistently with the more eroded experimental observations.

At the part load, the air fraction was still very low (fig. 18) but the vapour collapse took place in about $50\div 60$ [μs] that is in time intervals greater than the assumed critical limit (40 [μs]) reached at design flow rate. Furthermore, reducing the flow rate the warning zones shifted progressively towards the splitter tip as shown in fig. 19b by white spots.

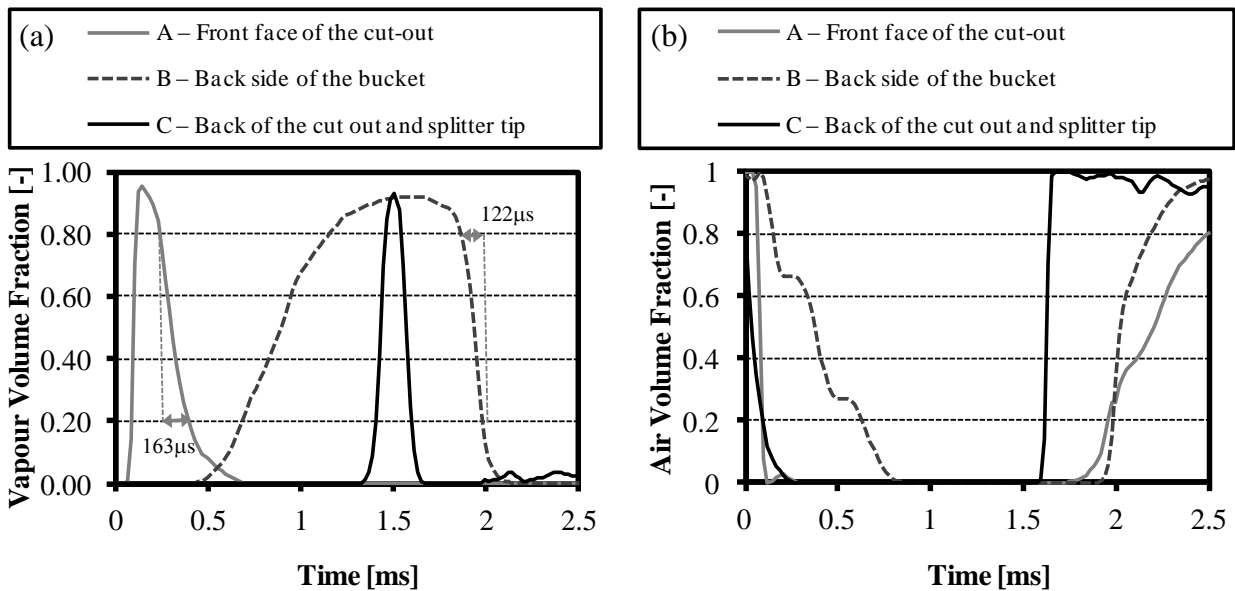


Fig. 18. Vapour (a) and air (b) volume fraction evolution for three points of fig. 6 ($Q = 50\% Q_{\text{Des}}$).

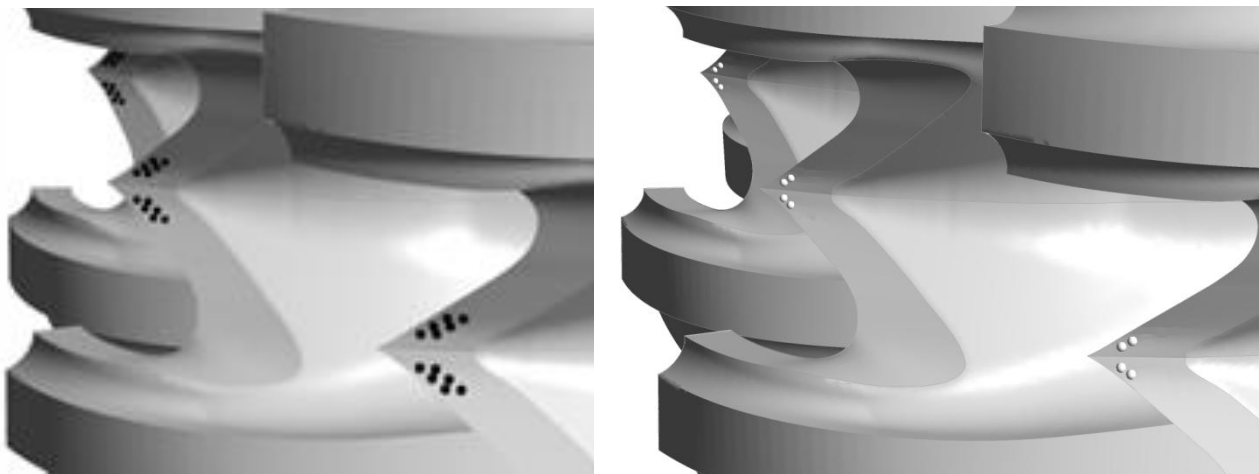


Fig. 19. Predicted points of damage in CFD analyses (a) at $100\% Q_{\text{Des}}$ and more critical zone (b) at 50% .

CONCLUSION

In this work a CFD based method was used to check the performance of a Pelton runner affected by pitting cavitation. The turbine was modelled and analyzed by unsteady RANS multiphase analyses considering water, water vapour and air.

Three different vapour volumes were located and the time evolution of the fractions of vapour and air was characterized both at design flow rate and at part load. The first vapour volume, placed on the bucket surface downstream the bucket cut-out, developed in the first phase of the cut in a sheet cavitation form and was due to high incidence angles between the water jet and the bucket surface. The second zone was characterized by large vapour volumes developed during the detachment of water jet from the back face of the bucket. This vapour volume moved with the water jet downstream the bucket, separated from the bucket surface back. The third volume was caused by the incidence angles of the flow with the cut-out back. It developed during the last steps of the cut in and showed an impulsive trend.

A direct analysis of bubbles inception, growth and collapse and the correlated damages could not be carried out economically on a full scale runner but the multiphase CFD analyses could be successfully used to gather information on Pelton cavitation mechanics. A simple procedure to identify the locations of higher damage risk was presented and verified on the test case runner. The post processing procedure was based on the time schedule of water, vapour and air on the bucket surface.

The filtering procedure was able to identify the critical area with a good precision when compared with the damaged zone on the real runner. It was also able to point out how the zones of higher risk of damage change with the flow rate.

The effectiveness of the defined tool required further enquiries but the preliminary analyses reported in this paper has highlighted its promising potential to study the impact of the geometrical parameters and configurations on the cavitation in Pelton.

REFERENCES

- [1] Tanaka H. 2000. Cavitation Phenomena in Hydraulic Machinery. In Li S C *Cavitation of Hydraulic Machinery* 211 - 228 Imperial College Press University of Warwick, U.K.
- [2] Iwai Y, and Okada T. 2000 Cavitation Damage to Hydraulic Machinery. In Li S C *Cavitation of Hydraulic Machinery* 269 - 258 Imperial College Press University of Warwick, U.K.
- [3] Grein H. 1990 *Cavitation pitting and rain erosion on Pelton runners* 5th IAHR Symposium on Hydraulic Machinery and Cavitation, Belgrade, Yugoslavia, September 11-14.
- [4] A. Perrig 2006 *Hydrodynamics of the free surface flow in Pelton turbine buckets* - PhD Thesis
- [5] Padhy, M. K., and R. P. Saini. 2012. Study of silt erosion mechanism in Pelton turbine buckets. *Energy* 39 (1) (3): 286-93.
- [6] Padhy, M. K., and R. P. Saini. 2011. Study of silt erosion on performance of a Pelton turbine. *Energy* 36 (1) (1): 141-7.
- [7] Avellan, F., Dupont, Ph., Kvicinsky, S. *Flow calculations in Pelton turbines—Part 2: free surface flows*. In: XIXth IAHR Symposium on Hydraulic Machinery and Systems, Singapore 1998.
- [8] Parkinson, E., Lestriez, R., Chapuis, L. 1998 *Flow calculations in Pelton turbines. Part 1 Repartitor and injector numerical analysis*. In Proceedings of the XIX IAHR Symposium, Singapore
- [9] Muggli, F., Zhang, Z. Schärer, C., Geppert, L. 2000 *Numerical and experimental analysis of Pelton turbine flow, Part 2 the free surface jet flow*. XX IAHR Symposium, Charlotte
- [10] Parkinson, E., Garcin, H., Vullioud, G., Muggli, F., Zhang, Z., Casartelli, E. 2002 *Experimental and numerical investigations of the free jet flow at a model nozzle of a Pelton turbine*. In Proceedings of the XXI IAHR Symposium on Hydraulic Machinery and Systems, Lausanne, Switzerland

- [11] Parkinson, E., Vullioud, G., Geppert, L., Keck, H. 2002 *Analysis of Pelton turbine flow patterns for improved runner component interaction*. Hydropower Dams (5)
- [12] Parkinson, E., Neury, C., Garcin, H., Vullioud, G., Weiss, Th. 2005 *Unsteady analysis of a Pelton runner with flow and mechanical simulations*. Hydro
- [13] Rossetti, A., Santolin, A., Cavazzini, G., Pavesi, G., Ardizzon G. 2011 *Analysis of a Pelton bucket efficiency*, 9th European Conference on Turbomachinery ; Istanbul, Turkey
- [14] Santolin, A., Cavazzini, G., Ardizzon, G., Pavesi, G. *Numerical investigation of the interaction between jet and bucket in a Pelton turbine* Proc. IMechE Part A: Journal of Power and Energy 2009 223: 721
- [15] ANSYS CFX-Solver Modeling Guide. *ANSYS CFX Release 12.0*.
- [16] Hammitt, F. G. 1963 *Observations on Cavitation Damage in a Flowing System*, Trans. ASME, J. Of Basic Engineering, pp. 3.
- [17] Wang, Y. C., Brennen, C.E. 1994 *Shock wave development in the collapse of a cloud of bubbles*, FED Vol 194, Cavitation and Multiphase flow, ASME 1994.
- [18] Fortes-Patella, R., Reboud, J.L., Briancon-Marjollet, L. 2004 *A phenomenological and numerical model for scaling the flow aggressiveness in cavitation erosion*, EROCAV Workshop, Val de Reuil.
- [19] Bark, G., Friesch, J., Kuiper, G., Ligtelijn, J.T. 2004 *Cavitation Erosion on Ship Propellers and Rudders*, 9th Symposium on Practical Design of Ships and Other Floating Structures, Luebeck-Travemuende, Germany.
- [20] Wang, Y.-C. 1996 *Shock waves in bubbly cavitating* - PhD Thesis.
- [21] Buttenbender, J. 2012 *Über die Dynamik von Kavitationswolken* - PhD Thesis.